Sensors and Materials, Vol. 35, No. 3 (2023) 975–987
MYU Tokyo

S & M 3222

Robust Co-registration of External Laser Altimetry Points and Stereo Images

Ruyan Zhou, Jinmeng Gao, Zhonghua Hong,* Haiyan Pan, Yun Zhang,Yanling Han, Jing Wang, and Shuhu Yang

College of Information Technology, Shanghai Ocean University,
999 Huchenghuan Road, Pudong New District, Shanghai, 201306, China

(Received December 28, 2022; accepted February 16, 2023)

Keywords: Gaofen-7, laser altimetry registration, combined adjustment, elevation positioning accuracy

Gaofen-7 (GF-7) is China's first submeter stereo mapping satellite, and the laser altimetry system equipped on it is used to improve its elevation positioning accuracy. The elevation positioning accuracy of GF-7 may be limited by the absence of a laser altimetry system. Therefore, it is necessary to study the combined adjustment of external laser altimetry points (LAPs) and GF-7 stereo images. In this study, we proposed a method consisting of registering LAPs to GF-7 stereo images followed by combined adjustment. The registration method adopts a coarse-to-fine scheme: the LAPs are reprojected to stereo images to obtain coarse coordinates, then fine coordinates are acquired by least-squares matching and using the epipolar geometry constraint. The proposed method can effectively improve the registration accuracy: the root mean square error (RMSE) of the registration is subpixel, compared with about three pixels when only random sample consensus (RANSAC) is applied. At the same time, the number of LAPs is also increased tenfold when using the proposed method. In the subsequent combined adjustment, the RMSE of the elevation positioning is decreased from about 5.5 to 1.3 m.

1. Introduction

As China's first submeter stereo satellite, Gaofen-7 (GF-7) has a wide range of applications such as natural hazard assessment, mapping, and so forth.[1,2] The elevation positioning accuracy can be improved using its equipped laser altimetry and footprint camera.[3–5] However, the ground resolution of its laser altimetry is relatively low, reaching 2.36 km in along-track scanning and 12.25 km[6] in cross-track scanning. Moreover, the altimetry echo wave may be invalid owing to clouds. As a result, the distribution of GF-7's laser altimetry points (LAPs) is not uniform, which has an adverse effect on its elevation positioning accuracy. Therefore, it is necessary to study the use of GF-7 stereo images in combination with external LAPs such as those obtained from the Ice, Cloud, and Land Elevation Satellites (ICESat-1, ICESat-2). External LAPs have also been used to improve the elevation positioning accuracy of stereo images. Li *et al.*[7] and Qv *et al.*[8] improved the elevation positioning accuracy of Ziyuan-3 (ZY-3) to 3 m using ICESat-1; the elevation positioning accuracy of ZY-3-02 was about 3.0 m after its

*Corresponding author: e-mail: zhhong@shou.edu.cn
https://doi.org/10.18494/SAM4288

ISSN 0914-4935

experimental laser altimetry data was used for adjustment,[9] and that of ZY-3-03 reached 2.58 m after combined adjustment using its synchronous laser altimetry data.[10]

However, ICESat-1 has a low spatial resolution, and some areas are not covered; thus, there are limitations in improving the elevation positioning accuracy of stereo images. ICESat-2 has a higher spatial resolution than ICESat-1; thus, the laser points of ICESat-2 are distributed more uniformly and densely than ICESat-1. However, ICESat-2 has a smaller diameter (17.5 m[11]) than ICESat-1 (70 m[12]), which means that ICESat-2 is more likely to be affected by the reprojection error of stereo images than ICESat-1. The image points obtained by directly reprojecting external LAPs onto stereo images using the rational function model (RFM)[13,14] are not corresponding points. They cannot be used in the subsequent steps because their coordinates in image space are different, which would lead to a considerable loss of positioning accuracy. Therefore, the main problem in combined adjustment using external LAPs and stereo images is the registration of LAPs.

The registration of external LAPs can be divided into two classes: registration based on topographic products and registration based on image matching. Registration based on topographic products such as a digital surface model (DSM) or a digital orthophoto map (DOM) is mainly performed to calculate the local minimum error between LAPs and the DSM[15,16] or DOM.[17] The inconsistency between LAPs and stereo images still exists if the DSM is not generated from stereo images to be used in the subsequent combined adjustment, which will introduce more sources of errors. It will also result in failure or misregistration if there is a very large difference in ground sample distance between the stereo images and the DSM. Image matching methods such as phase correlation[18–20] and least-squares matching (LSM)[21–23] are widely applied in the registration of images. However, image matching methods are easily affected by the quality of stereo images. For example, phase correlation is insensitive to the noise and illumination of stereo images, but it does not perform well in plain areas or areas with multiple similar peaks. Similarly, differences in the angle or level of radiation during imaging will lead to the failure of LSM. Moreover, the size of the search window in LSM has a significant impact on the registration result. Applying the RFM can reduce the search window size when LSM is conducted. However, registration errors inevitably remain because of the difference in the level of radiation between two stereo images with different imaging angles. Algorithms of elimination such as random sample consensus (RANSAC)[24] can be used to divide extracted feature points into inlier and outlier points to filter points containing registration errors. RANSAC is a robust algorithm that can obtain points with high accuracy. However, RANSAC often filters a large proportion of the points, which may result in an insufficient number of points for the following steps. Therefore, it is necessary to further study the registration methods of LAPs for stereo images.

To solve the above problems, in this paper, we propose a method of combining the adjustment of external LAPs with that of stereo images to improve the elevation positioning accuracy. First, the LAPs are registered to the stereo images. Then, based on the RFM of the stereo images, different types of points including tie points, LAPs, and virtual control points are used to construct error equations. Finally, the RFM is compensated, and its elevation positioning accuracy is improved.

The datasets of LAPs and stereo images and methods for the coarse-to-fine registration of external LAPs and combined adjustment are described in detail in Sect. 2, the results of registration and combined adjustment and several factors contributing to their performance are presented in Sect. 3, and conclusions on registration and combined adjustment are given in Sect. 4.

2. Materials and Methods

2.1 Materials

The data used in this study comprise GF-7 stereo images acquired in Luding, Sichuan, China, in November 2020, including four pairs of stereo images, i.e., eight stereo images. The latitude and longitude ranges are 29.348–30.22° and 101.96–102.394°, respectively. The resolutions of the forward (FWD) and backward (BWD) stereo images are 31268 × 31000 and 35864 × 40000 pixels, and their ground sample distances are about 0.8 and 0.65 m/pixel, respectively.

The LAPs used in this study were 668 points obtained from ICESat-2 in October 2018. To achieve uniformly distributed LAPs, half of them were used as elevation control points (ECPs), which were filtered by fixed longitude and latitude intervals, and the remaining LAPs were used as check points (CKPs).

The distribution of the ECPs and CKPs of GF-7 is shown in Fig. 1, and the date, number, spatial resolution, and coverage area of the datasets are presented in Table 1.

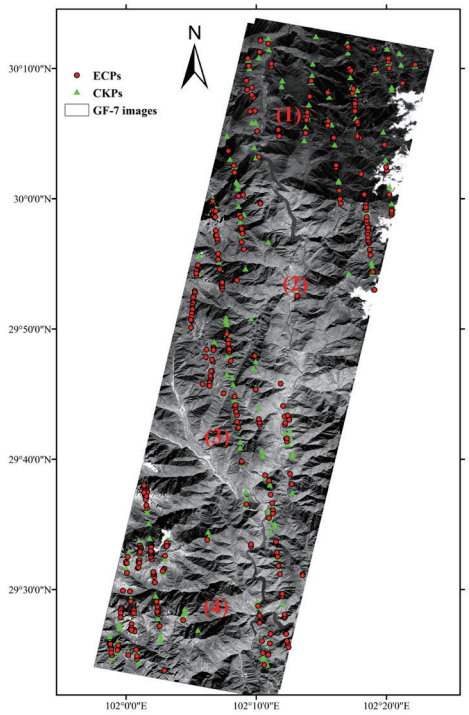

Fig. 1. (Color online) Distribution of GF-7 stereo images and external LAPs. ECPs: elevation control points; CKPs: check points.

Table 1
Data used in this paper.

Dataset	Date	Number	Spatial resolution (m)	Coverage area
GF-7 stereo images	May, June 2020	8	0.65–0.8	29.348–30.22N 101.96–102.394E
ICESat-2 ECPs	Oct. 2018	300	–100	29.348–30.22N 101.96–102.394E
ICESat-2 CKPs	Oct. 2018	368	–100	29.348–30.22N 101.96–102.394E

2.2 Methods

The improvement of the elevation positioning accuracy of stereo images is divided into two steps. As shown in Fig. 2, the LAPs are first registered to stereo images. The coarse-to-fine registration consists of three steps. First, LAPs are reprojected to two stereo images, with one treated as having fixed coordinates and the other treated as having coarse coordinates. Second, LSM is applied between the fixed and coarse coordinates. A homography matrix is built using the inlier points, and the best matrix is chosen as the epipolar geometry constraint, which is applied to constrain the outlier points. Third, combined adjustment is performed on the stereo images. The combined adjustment consists of three parts: the construction of compensation models, the construction of partial derivative terms based on the RFM, and the solution of error equations. The compensation model is constructed in a general affine manner, which has been found[25] to be effective for compensating the RFM. After the compensation model has been appended to the RFM, a Taylor expansion is applied in the compensation of the RFM. Partial derivatives concerning affine coefficients and coordinates of tie points in object space are constructed. Finally, error equations are constructed then solved, after which refined RFMs are generated.

2.2.1 Registration of LAPs

LAPs have high elevation positioning accuracy, but they cannot be directly used in stereo images because of the inconsistency between LAPs and stereo images. However, accurate coordinates are necessary, not only in object space but also in image space. To solve this problem, we propose a method of registering LAPs to stereo images. As shown in Fig. 3, the coarse-to-fine registration method is described as follows:

1) Reproject LAPs to stereo images to obtain coarse image coordinates (x_0, y_0), (x_1, y_1). Although both coordinates are inconsistent with the object of LAPs, it is feasible and reasonable to deem (x_0, y_0) as true and (x_1, y_1) as coordinates that contain errors.
2) Calculate the overlapping region of stereo images using the RFM and divide them into blocks to make it possible to apply LSM in each block.
3) Conduct LSM. Taking (x_0, y_0) as the center and 100 × 100 pixels as a block, slide the window that takes (x_1, y_1) as the center with 500 × 500 pixels as its area. The point (x_1, y_1) with the maximum correlation coefficient is taken as relatively fine image coordinates of LAPs. The formula used to calculate the correlation coefficient[26] is

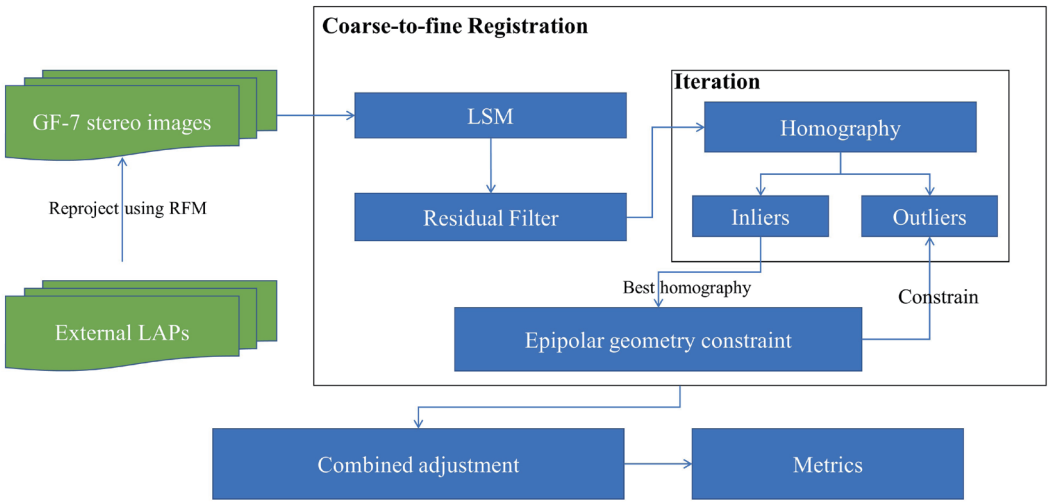

Fig. 2. (Color online) Framework of external LAP registration and improvement of elevation positioning accuracy of stereo images.

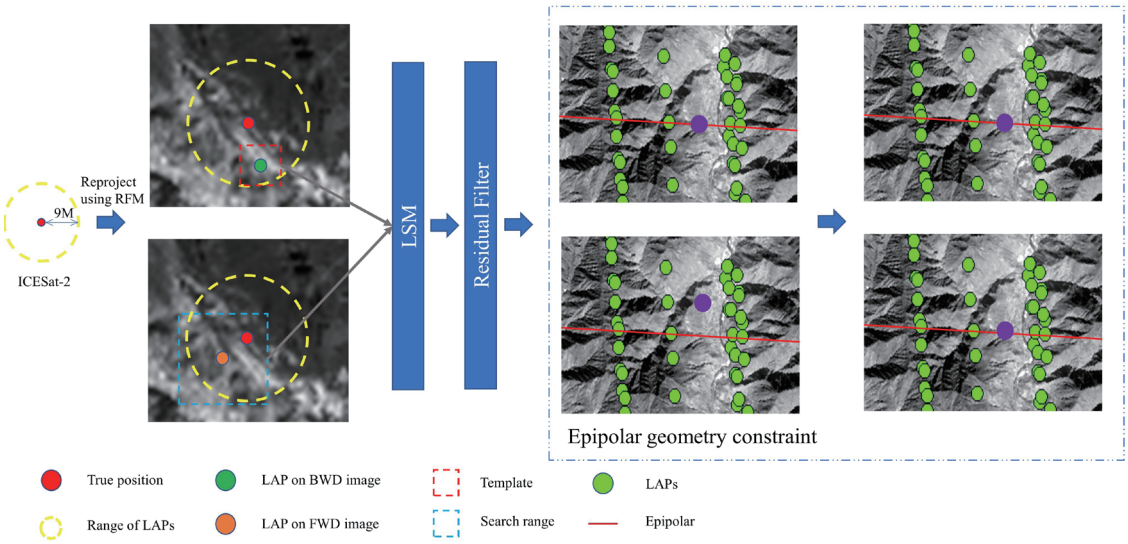

Fig. 3. (Color online) Registration of external LAPs.

$$\rho_{(x_2,y_2)} = \frac{\sum_{i=-\frac{h}{2}}^{\frac{h}{2}} \sum_{j=-\frac{w}{2}}^{\frac{w}{2}} \left(g_{(x_0+i,y_0+j)} - \overline{g}\right)\left(g'_{(x+i,y+j)} - \overline{g'}\right)}{\sqrt{\sum_{i=-\frac{h}{2}}^{\frac{h}{2}} \sum_{j=-\frac{w}{2}}^{\frac{w}{2}} \left(g_{(x_0+i,y_0+j)} - \overline{g}\right)^2 \sum_{i=-\frac{h}{2}}^{\frac{h}{2}} \sum_{j=-\frac{w}{2}}^{\frac{w}{2}} \left(g'_{(x+i,y+j)} - \overline{g'}\right)^2}}, \quad (1)$$

where w and h are the width and height of the search window, g and g' are the gray values of the windows on the BWD and FWD stereo images, and $\overline{g}$ and $\overline{g'}$ are the average gray values of the windows on the BWD and FWD stereo images, respectively.

4) However, image coordinates of LAPs inevitably contain errors after LSM because of the differences in the level of shadow or radiation in different stereo images. To solve this problem, we propose a filter using the RFM of stereo images. The filter consists of two parts: residual calculation and the construction of an epipolar geometry constraint. We calculate the residual from forward intersection and we reproject and reject residuals that are larger than three pixels. Then, we construct an epipolar geometry constraint to fit outlier LAPs. The forward intersection formula using the RFM is described as

$$\begin{cases} c_n^1 = \dfrac{Num_s\left(P_n, L_n, H_n\right)}{Den_s\left(P_n, L_n, H_n\right)} \\ r_n^1 = \dfrac{Num_L\left(P_n, L_n, H_n\right)}{Den_L\left(P_n, L_n, H_n\right)} \\ c_n^2 = \dfrac{Num'_s\left(P_n, L_n, H_n\right)}{Den'_s\left(P_n, L_n, H_n\right)} \\ r_n^2 = \dfrac{Num'_L\left(P_n, L_n, H_n\right)}{Den'_L\left(P_n, L_n, H_n\right)} \end{cases}, \tag{2}$$

where (P_n, L_n, H_n) and (c_n, r_n) are the normalized object and image coordinates of LAPs, respectively.

Then, we calculate the image coordinates (c_1', r_1') and (c_2', r_2') using (P_n, L_n, H_n) and the RFM. The residuals are obtained as

$$\begin{cases} r_c = c_1' - c_1 \\ r_r = r_1' - r_1 \end{cases}, \tag{3}$$

where r_c and r_r are the residuals of the columns and rows, respectively. The values larger than three pixels are rejected.

5) To further decrease the number of mismatched points, we apply the epipolar geometry constraint to the image coordinates of LAPs. The epipolar geometry constraint, such as the homography matrix, is described as

$$\begin{bmatrix} x_1 \\ y_1 \\ 1 \end{bmatrix} = \begin{bmatrix} h_{11} & h_{12} & h_{13} \\ h_{21} & h_{22} & h_{23} \\ h_{31} & h_{32} & h_{33} \end{bmatrix} \begin{bmatrix} x_2 \\ y_2 \\ 1 \end{bmatrix}, \tag{4}$$

where h_{11}–h_{33} are the coefficients of the homography matrix and can be calculated from the image coordinates of the LAPs. This method is used to update the homography matrix until it fits the largest number of image coordinates.

6) Finally, the LAPs that contain errors are corrected by the epipolar geometry constraint. The fine and corrected LAPs are applied in the following adjustment.

2.2.2 Combined adjustment

The RFM is a mathematical fitting form of a rigorous imaging model[13,14,27] given by Eq. (2), where r_n, c_n, P_n, L_n, and H_n represent the normalized stereo image row, column, longitude, latitude, and height calculated from the offset and scale, respectively, which can be easily acquired from a rational polynomial coefficient (RPC) file. Num_L, Den_L, Num_s, and Den_s represent the fitting form constructed from 20 coefficients of rows or columns, which can be found in the RPC file.

To reduce the errors generated in the push and sweep process of the satellite, different compensation models could be applied in the RFM. However, some researchers have demonstrated the effectiveness of the affine compensation model.[25] The affine compensation model is expressed as

$$\begin{aligned} \Delta r &= b_0 + b_1 c + b_2 r \\ \Delta c &= a_0 + a_1 c + a_2 r \end{aligned}, \tag{5}$$

where Δr and Δc represent the compensation terms of the rows and columns of stereo images, respectively. Terms with the subscript 0 represent the shifting errors, while terms with the subscripts 1 and 2 represent the rotation errors for columns and rows, respectively. Equation (5) was used to compensate Eq. (2) to obtain

$$\begin{cases} c_n = \dfrac{Num_s\left(P_n, L_n, H_n\right)}{Den_s\left(P_n, L_n, H_n\right)} + \Delta c \\ r_n = \dfrac{Num_L\left(P_n, L_n, H_n\right)}{Den_L\left(P_n, L_n, H_n\right)} + \Delta r \end{cases}. \tag{6}$$

To construct error equations, the Taylor expansion was applied to Eq. (6). Affine coefficients and the object of tie points were taken as the partial derivatives with respect to columns and rows. Terms with respect to longitude, latitude, and height comprise matrix $\boldsymbol{A}$, and terms with respect to coordinates of points in object space comprise matrix $\boldsymbol{B}$. Then, the Taylor expansion was appended to Eq. (6):

$$V = AX + BY - L, \tag{7}$$

where $\boldsymbol{V}$ represents the errors, $\boldsymbol{X}$ represents the compensation item of the affine coefficient, $\boldsymbol{Y}$ represents the compensation item of the object of points, $\boldsymbol{A}$ represents the partial derivatives of the compensation coefficient, and $\boldsymbol{B}$ represents the partial derivatives of the object of points. $\boldsymbol{A}$, $\boldsymbol{B}$, $\boldsymbol{X}$, and $\boldsymbol{Y}$ are described as

$$A=\begin{pmatrix} 0 & 0 & 0 & \frac{\partial r}{\partial b_0} & \frac{\partial r}{\partial b_1} & \frac{\partial r}{\partial b_2} \\ \frac{\partial c}{\partial a_0} & \frac{\partial c}{\partial a_1} & \frac{\partial c}{\partial a_2} & 0 & 0 & 0 \end{pmatrix}, \tag{8}$$

$$B=\begin{pmatrix} \frac{\partial r}{\partial P} & \frac{\partial r}{\partial L} & \frac{\partial r}{\partial H} \\ \frac{\partial c}{\partial P} & \frac{\partial c}{\partial L} & \frac{\partial c}{\partial H} \end{pmatrix}, \tag{9}$$

$$X=\begin{pmatrix} \Delta b_0 \\ \Delta b_1 \\ \Delta b_2 \\ \Delta a_0 \\ \Delta a_1 \\ \Delta a_2 \end{pmatrix} Y=\begin{pmatrix} \Delta P \\ \Delta L \\ \Delta H \end{pmatrix}. \tag{10}$$

Note that the longitude and latitude of LAPs must be compensated when the height is constrained as a fixed value.[27]

The following error equations are used in this paper:

$$\begin{cases} V_{tp} = A_{tp}X_{aff} + B_{tp}X_{tp} - L_{tp}, P_{tp} \\ V_{vcp} = A_{vcp}X_{aff} + B_{vcp}X_{vcp} - L_{vcp}, P_{vcp} \\ V_{las} = A_{las}X_{aff} + B_{las}X_{las} - L_{las}, P_{las} \end{cases}, \tag{11}$$

The terms with subscripts *tp*, *vcp*, and *las* denote the tie points, virtual control points, and LAPs, respectively. The compensation item must be updated when the maximum value of $\boldsymbol{X}$ and $\boldsymbol{Y}$ is greater than 10^{-8}.

3. Results and Discussion

We applied the proposed method to register external LAPs, which were used to improve the elevation positioning accuracy and decrease the inconsistency among stereo images. Experiments were divided into four image combinations, (1)–(4), as shown in Fig. 1.

To register the LAPs, the experiment was designed as follows: we calculated the matrix between the two sets of image coordinates, and we also calculated the residual by subtracting the coordinates calculated using the matrix from the coordinates in set 2.

The results of applying LSM only, RANSAC, and the proposed method are presented in Fig. 4. There are obvious errors in Fig. 4(a) due to the differences in the angle and level of radiation between the BWD and FWD stereo images, and the differences are too large to apply

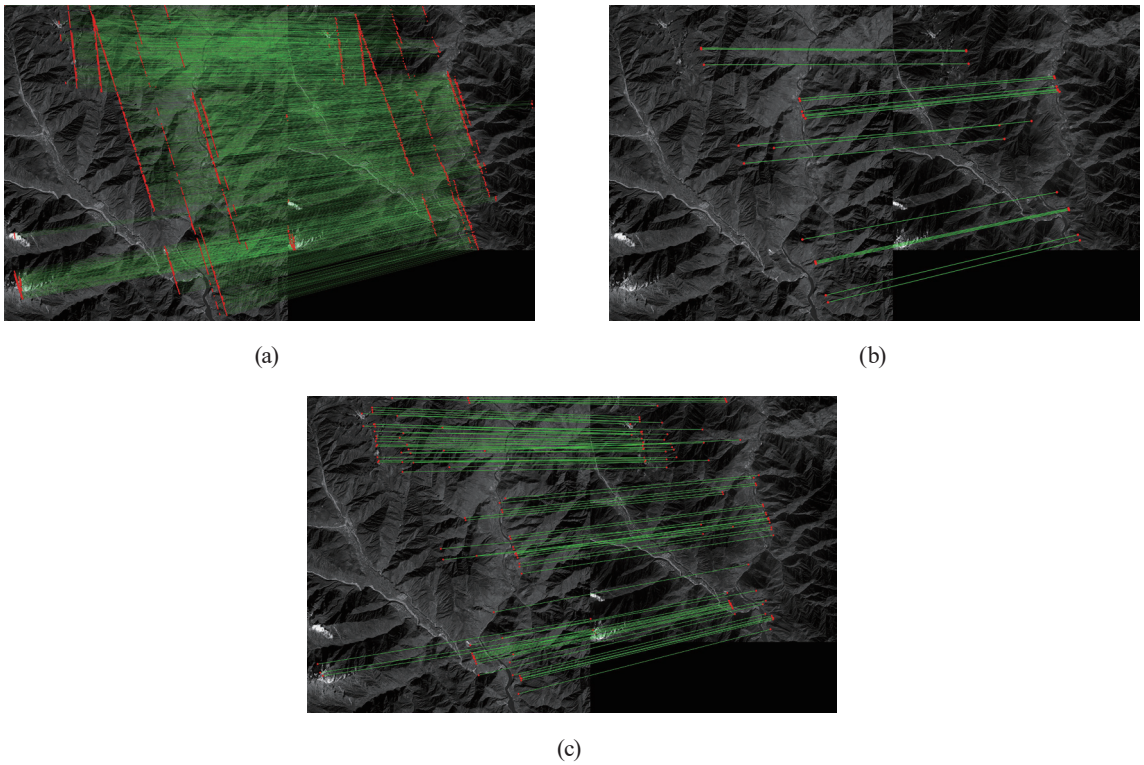

(a) (b)

(c)

Fig. 4. (Color online) Results of LAP registration: (a) applied LSM only, (b) RANSAC, and (c) proposed method.

LAPs in the subsequent combined adjustment. The number of LAPs significantly decreased when RANSAC was used, as shown in Fig. 4(b). After performing the coarse-to-fine registration proposed in this paper, the LAPs with better matching were saved, as shown in Fig. 4(c).

As can be seen from Table 2, when only LSM was applied to the four stereo images, all of them showed unsatisfactory experiment results: although all points were reserved, the root mean square error (RMSE) of two of the images reached a value above 840 pixels, one image had an RMSE of 146 pixels, and one image had an RMSE of 416 pixels, which were unacceptable errors for the subsequent steps. After RANSAC, the RMSE of the image coordinates of the LAPs significantly decreased to about four pixels. However, the number of LAPs also increased to about 20, which means that the retention rate was only 1%. A fatal flaw was that too few LAPs (less than 10) were reserved for the subsequent steps. In contrast, after filtering using the filter constructed using the RFM and epipolar geometry constraint proposed in this study, the RMSEs of the image coordinates of the LAPs decreased to less than one pixel, which means that the LAPs were sufficiently accurate to be applied in combined adjustment. At the same time, the retention rate reached 15%, ten times that obtained using RANSAC.

The LSM exhibited poor performance for two reasons. First, the stereo images used in this study mainly contained mountainous areas, making them easily affected by the inconsistency in the shadows resulting from the imaging angle when applying LSM. Second, the texture in mountainous areas showed weak and similar features, which is fatal for the gray-value-based matching method.

Table 2
Results of different LAP registration methods.

Image combination	Number	LSM only (pixels)		RANSAC (pixels)		Proposed method (pixels)	
		RMSE	REST	RMSE	REST	RMSE	REST
(1)	2800	416.166	2800	4.05221	20	0.649687	164
(2)	1266	951.804	1266	1.8088	15	0.857569	189
(3)	1216	146.8	1216	4.27161	18	0.225993	129
(4)	1931	849.247	1931	3.30734	24	0.62018	280

Table 3 shows the number of ECPs used in the experiment, the elevation accuracy, and the residual of the stereo images, including the RMSE, mid, and max values for different adjustment schemes. The table shows significant improvements in the elevation accuracy and residual of stereo images after the combined adjustment of LAPs and stereo images.

Generally, the RMSE elevation accuracy of stereo images improved from 5.5 to 1.3 m. The RMSE elevation accuracies of image combinations (1)–(4) increased from 5.45 to 1.37 m, from 5.52 to 1.58 m, from 5.04 to 1.26 m, and from 5.86 to 1.54 m, respectively.

Note that the elevation positioning accuracy of GF-7 is about 1 m after the combined adjustment, but the experimental results showed lower elevation positioning accuracy. This is because of the terrain in the stereo images: 90% of their area consisted of mountains, meaning that the LAPs were easily affected by the inconsistency between the LAPs and the stereo images. Therefore, small errors in the image coordinates (larger than one pixel) will cause very large losses in elevation positioning accuracy.

Before the combined adjustment, all image combinations showed similar elevation positioning accuracies, meaning that the four stereo image combinations showed an almost the same quality. After free network adjustment, the elevation positioning accuracy showed no apparent improvement, as expected. However, the different stereo image combinations showed different elevation accuracies, with stereo image combination (3) having the highest elevation accuracy and stereo image combination (2) having the lowest accuracy, with the other stereo image combinations showing similar elevation accuracies. Several factors contributed to this result, such as the LAPs used in the adjustment, the terrain, and the elevation positioning accuracy of the stereo images.

Although we have used the same number of ECPs in the experiment, other variables such as the co-registration accuracy, quality, and distribution of ECPs are difficult to control to be strictly consistent. The co-registration accuracy of LAPs is easily affected by the RFM of stereo images and the gray values of LAPs located in them. As a result, there is still some difference in the co-registration of LAPs, which will result in the difference in the elevation positioning accuracy of stereo images. Moreover, the distribution and quality of LAPs, which affect the elevation positioning accuracy of stereo images, cannot be changed. When the ECPs are distributed more uniformly, the improvement in the elevation positioning accuracy of stereo images generally shows more consistency. Finally, the quality of LAPs slightly differs even if they are filtered, which will further contribute to the nonconsistency in the experiments on the four image combinations.

Table 3
Results of different adjustment schemes.

Image combination	Adjustment scheme	No of ECPs	Height (m)			Residual (pixel)		
			MID	RMSE	MAX	MID	RMSE	MAX
(1)	Before adjustment	—	3.89	5.45	9.79	1.75	3.00	5.84
	Free network adjustment	—	3.88	5.44	9.78	0.48	0.62	0.82
	Adjustment with ICESat-2	75	1.30	1.37	4.00	0.48	0.63	0.82
(2)	Before adjustment	—	4.69	5.52	9.75	3.56	3.60	5.23
	Free network adjustment	—	4.83	5.53	9.4	1.28	1.29	4.07
	Adjustment with ICESat-2	75	1.36	1.58	1.76	1.00	1.25	2.04
(3)	Before adjustment	—	3.73	5.04	9.81	4.38	4.59	5.72
	Free network adjustment	—	8.10	4.60	9.40	1.01	1.18	1.76
	Adjustment with ICESat-2	75	1.04	1.26	2.86	0.98	0.96	1.76
(4)	Before adjustment	—	8.14	5.86	10.39	3.73	3.46	4.52
	Free network adjustment	—	9.33	5.28	10.84	0.29	0.39	0.90
	Adjustment with ICESat-2	75	2.28	1.54	4.54	0.23	0.39	0.90

As mentioned above, the terrain and elevation positioning accuracy of stereo images are important factors in the results. The more mountains or hills located in the stereo images, the greater the uncertainty in co-registration accuracy. The elevation positioning accuracy of stereo images under adjustment with or without LAPs exhibits the following relationship: image combinations with higher accuracies under free network adjustment are more likely to show higher accuracies after adjustment with LAPs. For example, among the four image combinations, image combination (4) showed the highest elevation positioning accuracy under the free network adjustment and also under the adjustment with ICESat-2.

There are also significant improvements in the residuals of the stereo images after combined adjustment: the RMSE residuals of image combinations (1)–(4) decreased from 3.00 to 0.63 pixels, from 3.60 to 1.25 pixels, from 4.59 to 0.96 pixels, and from 3.46 to 0.39 pixels, respectively. The decrease in stereo image residual means that the consistency between the image and object spaces of the stereo images is improved. The quality of the stereo image residual after adjustment depends on the tie points used in the experiment: the more uniformly the tie points are distributed, the greater the decrease in the residual obtained.

Several improvements remain to be made, such as those in the registration of LAPs, the retention rate of LAPs, and the elevation positioning accuracy. For the LSM, the template and search windows affect the registration, and the size of the windows should be adaptive to specific applications. The retention is low because the points acquired by the LSM inevitably contain errors owing to the quality or features of stereo images. The elevation positioning accuracy is affected by many factors, such as the quality of tie points, LAPs, and stereo images, which have a strict standard for the data accessed.

4. Conclusions

In this study, a new method of registering external LAPs to stereo images is proposed and used in the subsequent combined adjustment. In the method, ICESat-2 LAPs are registered to GF-7 stereo images. We performed experiments to demonstrate the effectiveness of the proposed method and obtained the following results:

(1) The proposed method significantly improved the registration accuracy, with the RMSE being reduced from about three pixels for RANSAC to less than one pixel. In addition, the proposed method reserved ten times the number of points as that obtained by the former method.

(2) The LAPs were then used to improve the elevation positioning accuracy of GF-7 stereo images. In the four stereo image combinations in this study, the RMSE of the elevation positioning error decreased from about 5.5 to 1.3 m, and that of the stereo image residual decreased from about four pixels to less than one pixel.

Acknowledgments

This work was supported in part by the National Natural Science Foundation of China under Grant 41871325.

References

1 H. Luo, B. He, R. Guo, W. Wang, X. Kuai, B. Xia, Y. Wan, D. Ma, and L. Xie: Remote Sens. **13** (2021) 3414. https://doi.org/10.3390/rs13173414
2 J. Wang, X. Hu, Q. Meng, L. Zhang, C. Wang, X. Liu, and M. Zhao: Remote Sens. **13** (2021) 4532. https://doi.org/10.3390/rs13224532
3 J. Chen, X. Tang, Y. Xue, G. Li, X. Zhou, L. Hu, and S. Zhang: Remote Sens. **14** (2022) 1666. https://doi.org/10.3390/rs14071666
4 C. Liu, X. Cui, L. Guo, L. Wu, X. Tang, S. Liu, D. Yuan, and X. Wang: Remote Sens. **14** (2022) 5868. https://doi.org/10.3390/rs14225868
5 C. Ren, J. Xie, X. Zhi, Y. Yang, and S. Yang: Sensors **20** (2020) 2319. https://doi.org/10.3390/s20082319
6 X. Tang, J. Xie, R. Liu, G. Huang, C. Zhao, Y. Zhen, H. Tang, and X. Dou: Earth Space Sci. **7** (2020) e2019EA000777. https://doi.org/10.1029/2019EA000777
7 G. Li, X. Tang, X. Gao, C. Zhang, and T. Li: Int. Arch. Photogramm. Remote Sens, Spat. Inf. Sci. **41** (2016) 37. https://doi.org/10.5194/isprsarchives-XLI-B1-37-2016
8 D. Qv, X. Tang, X. Zhu, and A. Li: 7th Symp. Novel Photoelectronic Detection Technology and Applications (SPIE, 2021) 1373–1378.
9 J. Xie, F. Hu, Z. Wang, M. He, Y. Zhen, and H. Zhu: 2019 IEEE Int. Geoscience and Remote Sensing Symp. (IGARSS 2019, IEEE, 2019) 3412–3415.
10 P. Zhou, X. Tang, D. Li, and X. Wang: IEEE Geosci. Remote Sens. Lett. **19** (2022) 1.https://doi.org/10.1109/LGRS.2022.3151473
11 B. Li, H. Xie, S. Liu, X. Tong, H. Tang, and X. Wang: Photogramm. Eng. Remote Sens. **87** (2021) 821. https://doi.org/10.14358/PERS.21-00009R2
12 B. E. Schutz, H. J. Zwally, C. A. Shuman, D. Hancock, and J. P. DiMarzio: Geophys. Res. Lett. **32** (2005). https://doi.org/10.1029/2005GL024009
13 C. V. Tao and Y. Hu: Photogramm. Eng. Remote Sens. **67** (2001) 1347.
14 J. Grodecki and G. Dial: Photogramm. Eng. Remote Sens. **69** (2003) 59. https://doi.org/10.14358/PERS.69.1.59
15 P. Gläser, I. Haase, J. Oberst, and G. Neumann: Planet. Space Sci. **89** (2013) 111. https://doi.org/10.1016/j.pss.2013.09.012
16 J. Zeng, J. Xie, R. Liu, F. Mo, and X. Yang: Remote Sens. **15** (2022) 62. https://doi.org/10.3390/rs15010062

17 X. Zhang, B. Xie, S. Liu, X. Tong, R. Ding, H. Xie, and Z. Hong: Remote Sens. **14** (2022) 4455. https://doi.org/10.3390/rs14184455
18 H. Xie, B. Li, X. Tong, X. Zhang, T. He, J. Dai, G. Huang, Z. Zhang, and S. Liu: IEEE Trans. Geosci. Remote Sens. **59** (2021) 9758. https://doi.org/10.1109/TGRS.2020.3048042
19 L. Liu, J. Xie, X. Tang, C. Ren, J. Chen, and R. Liu: Sensors **21** (2021) 2297. https://doi.org/10.3390/s21072297
20 N. Shorter and T. Kasparis: 2008 IEEE Int. Geoscience and Remote Sensing Symp. (IGARSS 2008, IEEE, 2008) 216–219.
21 Z. Li and J. Wang: ISPRS Ann. Photogramm. Remote Sens. Spatial Inf. Sci. **2** (2014) 37. https://doi.org/10.5194/isprsannals-II-1-37-2014
22 R. Zhou and W. Jiang: Remote Sens. **12** (2020) 2163. https://doi.org/10.3390/rs12132163
23 C. Liu, X. Tang, H. Zhang, G. Li, X. Wang, and F. Li: IEEE Geosci. Remote Sens. Lett. **19** (2021) 1. https://doi.org/10.1109/LGRS.2021.3136389
24 J. Li, Q. Hu, and M. Ai: IEEE Trans. Geosci. Remote Sens. **59** (2021) 9716. https://doi.org/10.1109/TGRS.2020.3045456
25 X. Tong, Z. Hong, S. Liu, X. Zhang, H. Xie, Z. Li, S. Yang, W. Wang, and F. Bao: ISPRS J. Photogramm. Remote Sens. **68** (2012) 13. https://doi.org/10.1016/j.isprsjprs.2011.12.004
26 S. Kaneko, Y. Satoh, and S. Igarashi: Pattern Recognit. **36** (2003) 1165. https://doi.org/10.1016/S0031-3203(02)00081-X
27 X. Tang, C. Liu, P. Zhou, N. Cao, F. Li, and X. Wang: Photogramm. Eng. Remote Sens. **86** (2020) 215. https://doi.org/10.14358/PERS.86.4.215